On the propagation of blobs in the magnetotail: MHD simulations

J. Birn,[1,2] R. Nakamura,[3] and M. Hesse[4]

Received 5 June 2013; revised 23 July 2013; accepted 16 August 2013; published 6 September 2013.

[1] Using three-dimensional magnetohydrodynamic (MHD) simulations of the magnetotail, we investigate the fate of entropy-enhanced localized magnetic flux tubes ("blobs"). Such flux tubes may be the result of a slippage process that also generates entropy-depleted flux tubes ("bubbles") or of a rapid localized energy increase, for instance, from wave absorption. We confirm the expectation that the entropy enhancement leads to a tailward motion and that the speed and distance traveled into the tail increase with the entropy enhancement, even though the blobs tend to break up into pieces. The vorticity on the outside of the blobs twists the magnetic field and generates field-aligned currents predominantly of region-2 sense (earthward on the dusk side and tailward on the dawn side), which might provide a possibility for remote identification from the ground. The breakup, however, leads to more turbulent flow patterns, associated with opposite vorticity and the generation of region-1 sense field-aligned currents of lower intensity but approximately equal integrated magnitude.

Citation: Birn, J., R. Nakamura, and M. Hesse (2013), On the propagation of blobs in the magnetotail: MHD simulations, *J. Geophys. Res. Space Physics*, *118*, 5497–5505, doi:10.1002/jgra.50521.

1. Introduction

[2] Entropy-depleted magnetic flux tubes in the magnetotail ("bubbles") [*Pontius and Wolf*, 1990; *Chen and Wolf*, 1993; *Birn et al.*, 2004; *Wolf et al.*, 2009] have been identified as the major mechanism of earthward transport of magnetic flux, particles, and energy, closely associated with fast earthward plasma flows ("bursty bulk flows" or BBFs) [e.g., *Baumjohann et al.*, 1990; *Angelopoulos et al.*, 1992, 1994; *Sergeev et al.*, 1996; *Schödel et al.*, 2001a, 2001b; *Petrukovich et al.*, 2001]. A common measure for the entropy in approximate equilibrium is the quantity pV^γ [e.g., *Wolf et al.*, 2009], where $\gamma = 5/3$ is the ratio of specific heats for an isotropic ideal gas, and

$$V = \int \mathrm{d}s/B \tag{1}$$

is the volume of a magnetic flux tube of unit magnetic flux, integrated over the length of the flux tube. In nonequilibrium situations, when the pressure p is not constant on field lines, it is useful to replace the quantity $p^{1/\gamma}V$ by [e.g., *Birn et al.*, 2009]

$$S = \int p^{1/\gamma}\,\mathrm{d}s/B \tag{2}$$

The quantity S is conserved in ideal magnetohydrodynamics (MHD) when losses from the flux tube are negligible. It becomes a direct measure of entropy when the flux tube relaxes into equilibrium.

[3] The most plausible cause for depleted flux tubes and BBFs in the magnetotail is spatially and temporally localized reconnection [e.g., *Sergeev et al.*, 1992; *Nagai et al.*, 1998; *Øieroset et al.*, 2000; *Shay et al.*, 2003; *Forsyth et al.*, 2008], which not only severs and ejects some part of the closed flux tubes as a plasmoid [*Hones*, 1977] but also causes a collapse of the shortened flux tubes in the inner tail and generates fast flows. Potential alternative formation processes include the loading of flux tubes with preexisting reduced entropy content, entropy losses to the ionosphere, or a diffusion/slippage process in the tail [*Wolf et al.*, 2009], the presumed consequence of current disruption by microinstabilities that break the frozen-in condition of ideal MHD but may not necessarily lead to topological reconnection [e.g., *Lui et al.*, 1992]. Regardless of the mechanism of loss, the entropy reduction was found to be crucial in the earthward transport and the depth of penetration to Earth, both in observations [*Yang et al.*, 2010a; *Dubyagin et al.*, 2011] and magnetohydrodynamic (MHD) simulations [*Birn et al.*, 2004, 2009].

[4] As pointed out by *Wolf et al.* [2009] and *Yang et al.* [2010b], a slippage process that causes entropy reduction on its earthward side should also lead to an entropy enhancement on the tailward side, resulting in the formation of a "blob" [*Pontius and Wolf*, 1990]. *Yang et al.* [2010b] investigated the evolution of an artificially generated bubble-blob pair using the Rice Convection Model (RCM-E), based on the assumption of instantaneous equilibrium. They found the expected earthward motion of the bubble and tailward motion of the blob, together with the formation of a thin

[1]Space Science Institute, Boulder, Colorado, USA.
[2]Also guest scientist at Los Alamos National Laboratory, Los Alamos, New Mexico, USA.
[3]Space Research Institute, Austrian Academy of Sciences, Graz, Austria.
[4]NASA/Goddard Space Flight Center, Greenbelt, Maryland, USA.

Corresponding author: J. Birn, Space Science Institute, 4750 Walnut Street, Suite 205, Boulder, CO 80301, USA. (jbirn@lanl.gov)

2169-9380/13/10.1002/jgra.50521

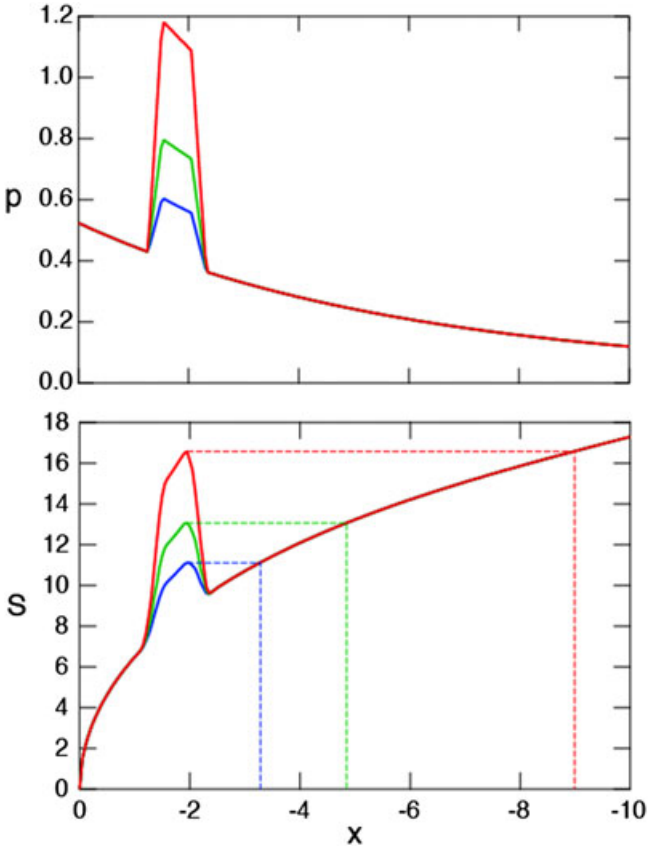

Figure 1. Initial perturbation of (top) pressure and (bottom) entropy function S along the x axis for 3 different values f of temperature enhancement. The dashed lines indicate an estimate for the propagation distance.

current sheet in between, which they argued should enable the onset of reconnection. An earthward/tailward moving pair of bubble and blob was also found in a global MHD simulation of a substorm, associated with a local stretching and thinning, which triggered explicit localized resistivity in the code [*Hu et al.*, 2011; *Zhu et al.*, 2013].

[5] In these models the formation of a bubble-blob pair is closely related to a local violation of ideal MHD, resulting in entropy diffusion and antidiffusion [*Lee et al.*, 1998]. An alternative mechanism of blob formation might be the resonant absorption of energy within a particular flux tube. This mechanism was investigated by *Smith et al.* [1986] and *Goertz and Smith* [1989], who suggested that the catastrophic enhancement of the energy absorption of Alfvén waves in the plasma sheet boundary layer could lead to sudden local heating and the initiation of substorm onset.

[6] It should be noted that the terminology of entropy-depleted bubbles and entropy-enhanced blobs, as introduced by *Pontius and Wolf* [1990] and now commonly used, is opposite to that of *Goertz and Baumjohann* [1991]. Using an analogy between Lorentz forces and gravity in balancing pressure gradient forces, the latter would seem more appropriate. However, the Pontius-Wolf notation has become common and will be used here.

[7] In this paper we investigate the consequences of the formation of a blob in the magnetotail, disregarding the actual mechanism of formation. Three-dimensional MHD simulations of bubble propagation have shown that vorticity near the front of an earthward flow leads to the formation of a field-aligned current system of region 1 sense (earthward on the dawnward edge, tailward on the duskward edge) [*Birn et al.*, 2004], consistent with observed near-Earth signatures of flow bursts related to auroral streamers [e.g., *Fairfield et al.*, 1999; *Lyons et al.*, 1999; *Zesta et al.*, 2000; *Nakamura et al.*, 2001a 2001b; *Sergeev et al.*, 2004; *Grocott et al.*, 2004]. Similar consequences might be expected from vorticity surrounding a tailward moving blob.

[8] We note here that our approach is based on the approximation of ideal MHD and the conservation of specific entropy. This approach obviously is questionable when the formation of a blob is caused by field line slippage from a violation of the flux conservation of ideal MHD, whereas

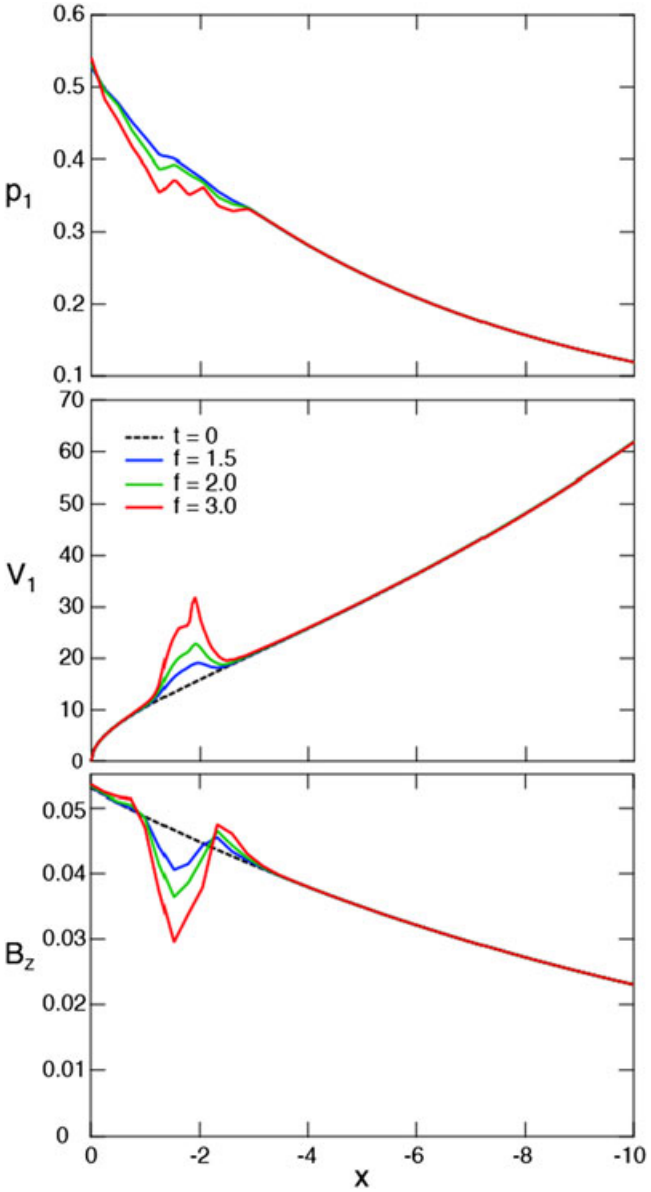

Figure 2. Variation of (top) pressure p, (middle) flux tube volume V, and (bottom) B_z along the x axis after 1 Alfvén time. The dashed lines in Figures 2(middle) and 2(bottom) represent the initial distributions.

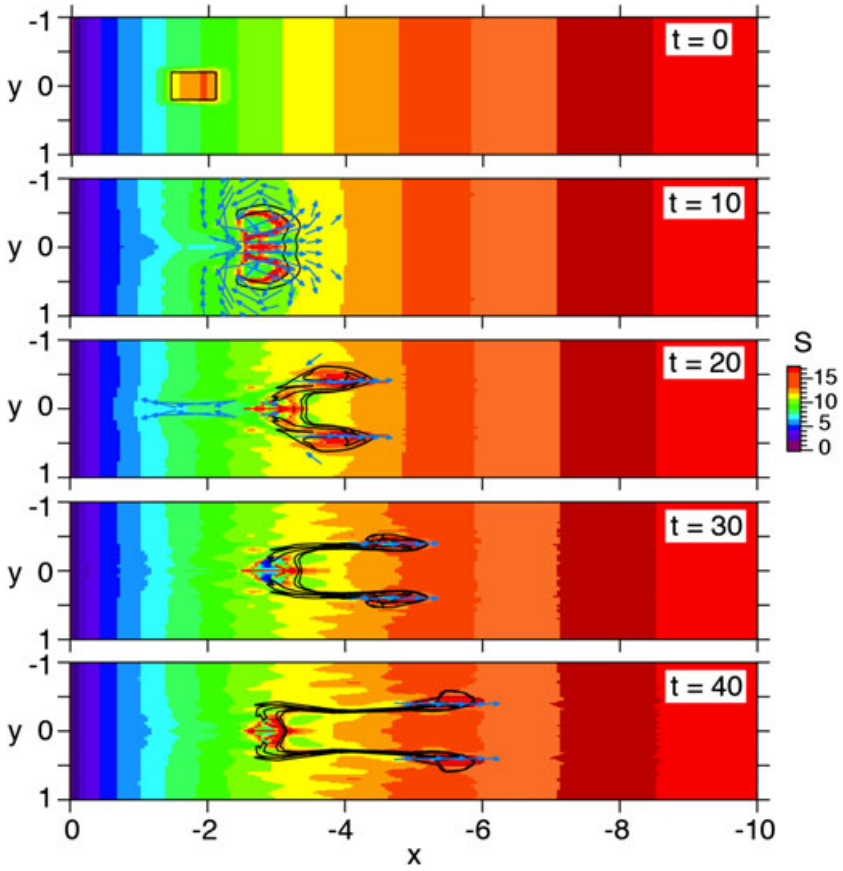

Figure 3. (top–bottom) Evolution of an entropy-enhanced flux tube with $f = 2$ in the equatorial plane. Color shows the entropy integral S defined by (2) and blue arrows represent velocity vectors with a magnitude above 0.05 (50 km/s). The black contours show the distorted boundary of the initially enhanced area (dashed line in Figure 3, top) propagated by the flow.

it may be more defensible in the case of a sudden energy absorption. The reason for this approach is that we deliberately wanted to avoid the onset of tearing or reconnection to study the properties of a tailward moving flux rope that remains connected with Earth, as opposed to a detached plasmoid.

2. Overview of the Numerical Procedure

2.1. Initial State

[9] We use the same initial magnetic field configuration as in previous studies of earthward propagating bubbles [*Birn et al.*, 2004]. It is given by a self-consistent two-dimensional equilibrium [*Fuchs and Voigt*, 1979; *Chen and Wolf*, 1999], through a flux function

$$A(x,z) = -\frac{1}{\alpha}\sin[\alpha(|z|-1)]\exp(\alpha x) \qquad \text{for } |z| > 1 \tag{3}$$

$$A(x,z) = \frac{2}{\pi}\cos\left(\frac{\pi}{2}z\right)\exp(\alpha x) \qquad \text{for } |z| \le 1 \tag{4}$$

with $\alpha = 0.0816$ and $\mathbf{B} = \nabla A \times \hat{\mathbf{y}}$. A coordinate frame is used with x negative down tail, y pointing duskward and z northward. The unperturbed plasma pressure is given by

$$p = p_0 \qquad \text{for } |z| > 1 \tag{5}$$

$$p = p_0 + \frac{A^2}{2}\left[\left(\frac{\pi}{2}\right)^2 - \alpha^2\right] \qquad \text{for } |z| \le 1 \tag{6}$$

The initial, unperturbed, temperature is assumed uniform such that the density is proportional to the pressure. A uniform background density and corresponding pressure, $p_0 = 0.025$, are included to keep the density and Alfvén speed finite in the lobe regions $|z| > 1$.

[10] We use normalized quantities based on characteristic units, which may be taken in agreement with *Chen and Wolf* [1999]: the plasma sheet or current sheet half-width L (taken as 4 R_E), the magnetic field strength for $z = 1$ at the earthward boundary of the simulation box, B_L (37.5 nT), and a characteristic Alfvén speed of 1000 km/s. This leads to a pressure unit B_L^2/μ_0, and a time unit of ~25 s. The box size is given by $0 \ge x \ge -10$, $|y| \le 2$, and $0 \le |z| \le 2$, using (mostly) symmetry around $y = 0$ and $z = 0$.

2.2. Code

[11] The blob evolution is obtained by integrating the dynamic MHD equations, using an explicit finite-difference scheme [*Birn et al.*, 1996, 2004] with nonuniform grid in z, such that about 1/2 of the grid points lie within the plasma sheet. A quasi-viscous term, similar to flux-corrected transport algorithms [e.g., *Book et al.*, 1975] is added to damp oscillations on the grid scale, and to increase numerical stability. This algorithm is not used on the magnetic field to avoid artificial diffusion and reconnection. Energy transport and conversion are governed by an adiabatic law with a ratio

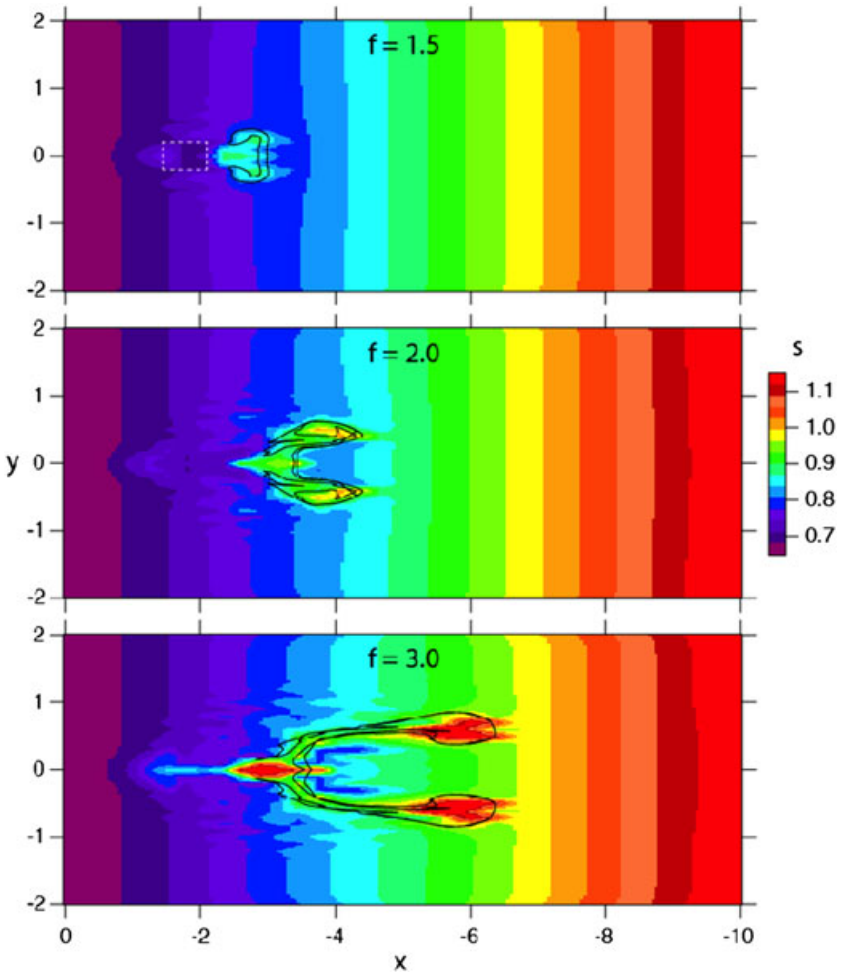

Figure 4. Effect of the entropy enhancement on the blob propagation. Color shows the specific entropy, measured by $s = p^{1/\gamma}/\rho$, in the equatorial plane at $t = 20$ for three different values of f, The black contours show the distorted boundary as advanced by the flow.

of specific heats $\gamma = 5/3$. For the runs presented, the number of grid cells in x, y, and z, were 64, 40, and 64, respectively, for the full box. By varying the grid size and the time step, we confirmed that the basic results reported here are not affected significantly by the spatial or temporal resolution, as shown in Appendix A. Frozen-in ($\mathbf{v} = 0$) boundary conditions were used at $x = 0$ and $|y| = y_{max}$, $|z| = z_{max}$ with Von Neumann conditions ($\partial/\partial n = 0$) for density and pressure, whereas a free-outflow condition was imposed at $x = -10$.

3. Initiation

[12] The evolution is initiated by a perturbation consisting of a temperature (and pressure) enhancement by a factor f of 1.5–3 on a flux tube defined by unperturbed pressure values $0.375 < p < 0.425$, crossing $z = 0$ between $x = -1.3$ and $x = -2.2$, with $|y| \leq 0.2$. Figures 1(top) and 1(bottom) show the initial pressure and the entropy function (2) along the x axis for three different values of f. The dashed lines in Figure 1(bottom) represent the locations where the unperturbed value of S matches that of the maximum within the blob, providing an estimate for the expected travel distance.

[13] The initial pressure enhancement results in a force imbalance of the enriched flux tube with the surrounding medium. As demonstrated by Figure 2, this becomes adjusted within approximately 1 Alfvén time, such that the pressure approaches the neighboring unperturbed pressure. Due to the conservation of entropy (2), the flux tube volume V increases in the perturbed flux tube, and correspondingly, the magnetic field at the equatorial plane decreases. The pressure reduction also leads to a density and temperature reduction, although the temperature remains increased above that of the surrounding medium.

4. Blob Propagation

[14] Figure 3 shows the propagation of a blob in the equatorial plane for an initial temperature enhancement by a factor $f = 2$. Color shows the entropy integral S in the x,y plane, together with velocity vectors (blue arrows) with a magnitude above 0.05 (80 km/s). Black contours show the distorted boundary of the initially enhanced area (Figure 3,top) as propagated by the flow. The tailward motion of the blob generates twin vortices, which distort the initial cross section and eventually cause a breakup of the blob into two parts off the midnight plane. These parts continue the tailward motion while the central part stops and even moves back slightly earthward.

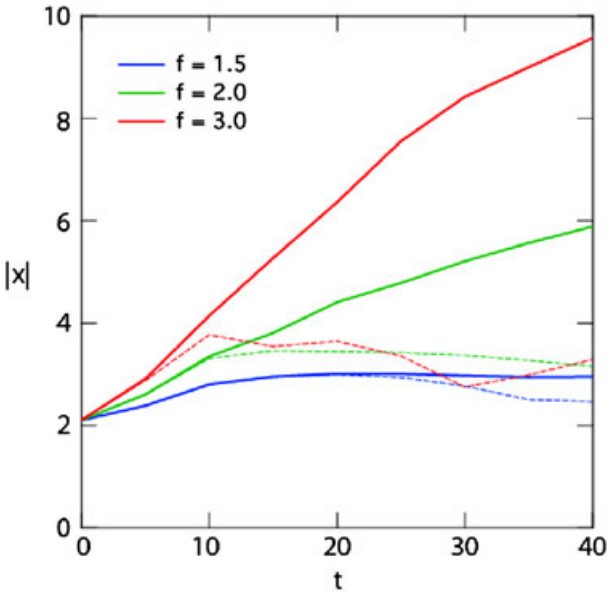

Figure 5. Propagation of the front (solid lines) and center (dashed lines) of blobs as function of time for three different values of f.

[15] The tailward motion, speed and distance of propagation, depend strongly on the amount of entropy enhancement. This is demonstrated by Figure 4, which shows the specific entropy, measured by $s = p^{1/\gamma}/\rho$, in the equatorial plane at $t = 20$ for three different values of initial temperature enhancement f. Black contours again show the propagated distorted boundary of the initial blob cross section. Figure 4 shows that the speed and distance traveled increase with the amount of entropy enhancement. Furthermore, the winding and the associated distortions by the vortical flow also increase with the amount of entropy enhancement. Ideally, the regions of enhanced specific entropy should be confined within the distorted boundaries. However, there is some entropy diffusion resulting from the finite grid resolution, which does not resolve the finely wound-up structure.

[16] Figure 5 demonstrates the propagation of the front and center of the blobs for three different values of f. The solid lines represent the farthest distance in $|x|$ of a blob part, obtained from the distorted boundaries, and the dashed lines the distance at $y = 0$. The central portion comes to rest after about 10 Alfvén times, whereas the outer portions travel to distances commensurate with those estimated from Figure 1(bottom) on the basis of entropy balance with the surrounding unperturbed medium.

5. Field-Aligned Currents

[17] The vortex motion illustrated in Figure 3 indicates a twisting of the associated magnetic flux tubes, which should lead to a build-up of field-aligned currents. This is confirmed by evaluating $J_{\|}$ at the near-Earth boundary. Figure 6 shows the x component of $J_{\|}$ (which is almost identical to $J_{\|}$) for two values of f at three different times. Red color corresponds to earthward and blue color to tailward directed currents. The dominant structure thus represents region-2 type currents as expected from the vortical motion. However, on the outside of the main currents, there are also currents of opposite sense (region-1 type), which tend to become stronger at later times. The more strongly enriched flux tube ($f = 3$) even shows a breakup of the field-aligned currents into multiple systems at $t = 30$, presumably associated with a more turbulent breakup of the flows surrounding the blob.

[18] The rise of the maximum and the total integrated field-aligned currents of region-1 and region-2 type is

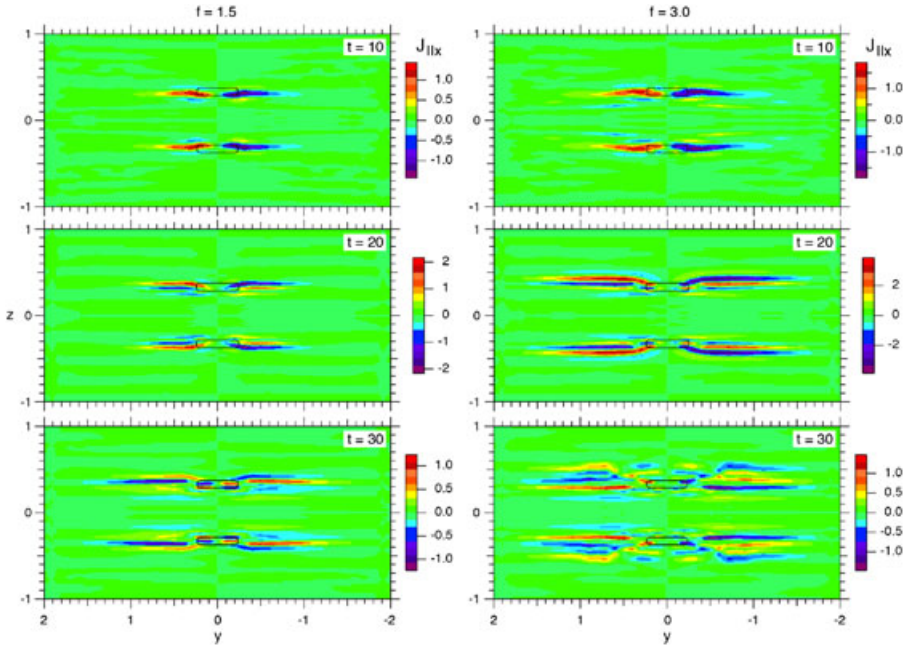

Figure 6. Field-aligned currents $J_{\|x}$ (color) at the inner boundary $x = 0$ for two cases of entropy enhancements with (left) $f = 1.5$ and (right) $f = 3.0$ for three different times. The black contours outline the cross section of the flux tube with enhanced entropy.

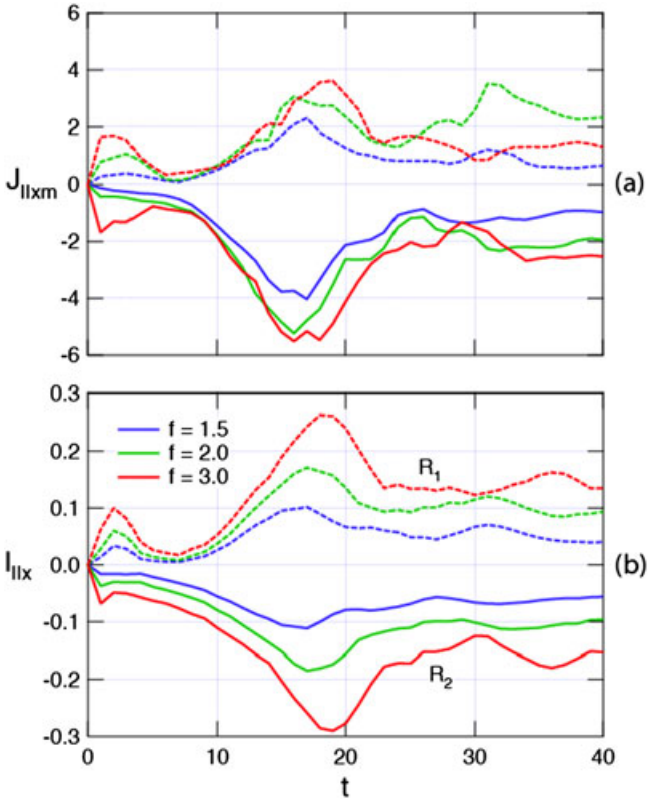

Figure 7. Temporal evolution of field-aligned currents at the near-Earth boundary $x = 0$ for $y < 0, z > 0$ and three values of f, (a) maximum and minimum current density $J_{\|x}$, and (b) total integrated current of region-1 and region-2 type.

demonstrated by Figure 7. Figure 7a shows the maximum and minimum values of $J_{\|x}$ at $x = 0$ obtained for $y < 0$ with positive values corresponding to region-1 type and negative values to region-2 type. Figure 7b shows the integrated currents of region-1 ($I_{\|x} > 0$) and region-2 type ($I_{\|x} < 0$), respectively. The peak values of current density show the dominance of region-2 type currents, but somewhat surprisingly, the integrated currents of the two types almost balance, particularly at later times and larger values of f. This is not obvious from Figure 6 except for the late stage of $f = 3$; it is due to the fact that the region-1 type currents surrounding the region-2 type currents are more widely spread out.

6. Summary and Discussion

[19] Using three-dimensional ideal MHD simulations, we have investigated the propagation of entropy-enhanced magnetic flux tubes (blobs) in the magnetotail. In analogy to earthward moving bubbles, the blobs move tailward at speeds and for distances that depend strongly on the amount of entropy increase. The distance traveled agrees well with the expectation from entropy balance with the surrounding unperturbed medium. However, we note that the imposed field line tying at the near-Earth boundary prevents the blob flux tubes from assuming a location where their entropy and pressure exactly matches the surrounding medium.

[20] The blobs tend to break up into (here) two pieces, such that a central portion stops at a short distance while the outer portions travel the expected distance based on the entropy argument. However, this is not a universal feature; it apparently depends on the shape of the entropy-enhanced flux tube. In a comparison run with a blob of initially elliptical cross section in the equatorial plane, the blob also showed the rotation and folding of its outer parts, but the two parts stayed closer together, so that the subsequent propagation was more like that of a united blob.

[21] The tailward flow generates twin vortex motions on the outside, which not only distort the initial blob boundary but also cause a twisting of the surrounding magnetic flux tubes and thereby a build-up of field-aligned currents of region-2 sense (tailward on the dawnside and earthward on the duskside. These currents map to the earthward boundary and could possibly provide observable ionospheric signatures, analogous to those of earthward propagating bubbles. The mechanism for the field-aligned current generation is illustrated by Figure 8, which provides a perspective view of field-aligned current density (color) at $x = 0$ together with flow vectors and the specific entropy (color) $s = p^{1/\gamma}/\rho$ in the equatorial plane for a run with $f = 2$ at $t = 15$. The blue and red contours in the $z = 0$ plane are mapped by field lines from contours $j_{\|x} = \pm 1.5$ at $x = 0$. Two field lines (heavy red and blue lines) from the tailward current region illustrate the twist or shear caused by the flow. The run also contained an initial cross-tail field component on 1% of the main field, which causes a slight asymmetry in the field-aligned currents at $x = 0$ and the mapped contours at $z = 0$ but has otherwise no significant effect on the evolution.

[22] The twisted flux rope carrying the enhanced field-aligned current at $x = 0$ does not map to the region of enhanced vorticity. That is not surprising because the

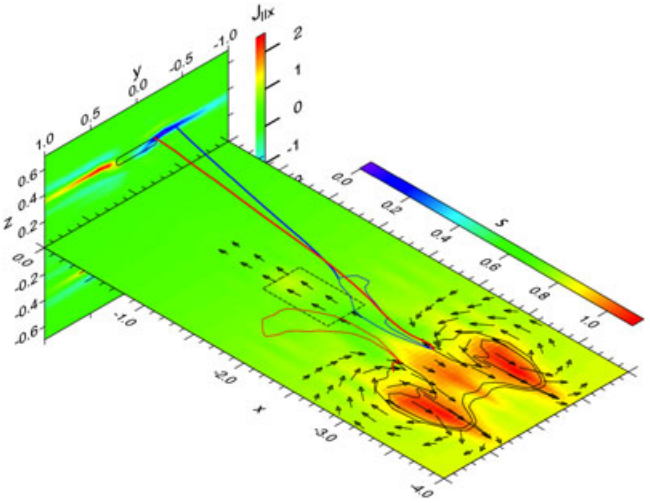

Figure 8. Perspective view of the connection between a tailward propagating blob and the buildup of field-aligned currents at $t = 15$ for a run with $f = 2$. The vertical plane $x = 0$ shows the magnitude of the x component of $J_{\|x}$ (color) and the outline of the bubble cross section. The horizontal plane $z = 0$ shows the specific entropy $s = p^{1/\gamma}/\rho$ in color together with flow vectors and the distorted blob boundary. The dashed line indicates the initial cross section of the blob in the equatorial plane. The blue and red contours in the $z = 0$ plane are mapped by field lines from contours $j_{\|x} = \pm 1.5$ at $x = 0$. Two such field lines are indicated by heavy lines.

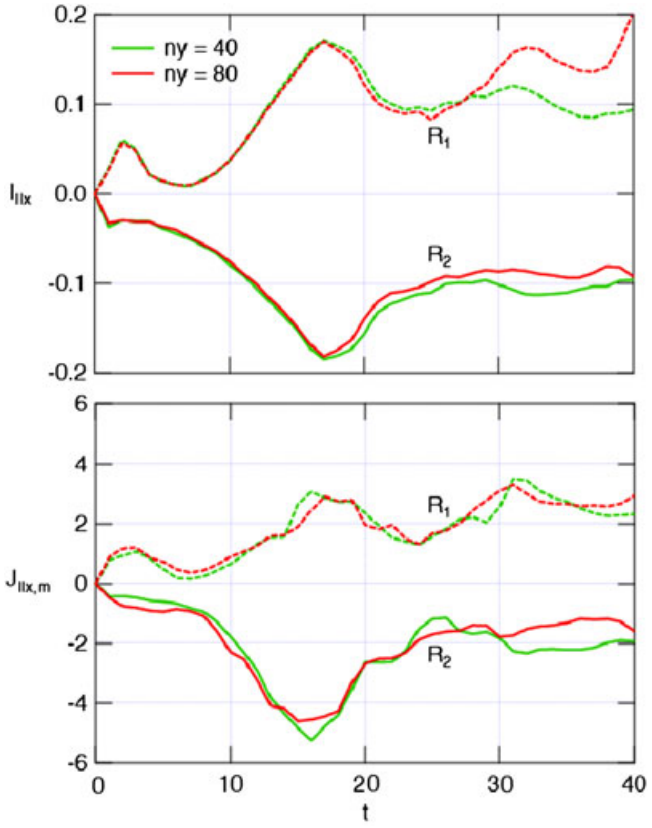

Figure A1. Temporal evolution of field-aligned currents at the near-Earth boundary $x = 0$ for $f = 2$ and different resolution in y, (a) maximum and minimum current density $J_{\|x}$, and (b) total integrated current of region-1 and region-2 type.

twisting is caused by the history of vortex flow, not by the instantaneous vorticity. We also note that the enhanced field-aligned currents at $x = 0$ are not contained within the flux rope mapped to the equatorial plane. This is due to the presence or even dominance of perpendicular currents, such that field-aligned currents are not conserved by themselves, except close to Earth where they become the dominant currents. The mapping of field-aligned currents from Earth therefore does not necessarily accurately indicate the source region, even if the magnetic field were known perfectly.

[23] In addition to the dominant region-2 type field-aligned currents, the simulations show the development of region-1 type currents on the outside, which are lower in peak density but almost equal in integrated magnitude. For strong entropy enhancement and at later times, the field-aligned currents tend to break up into multiple filaments.

[24] Entropy enriched magnetic flux tubes might be the consequence of a diffusion/slippage process, violating ideal MHD, which generates both entropy-depleted (bubbles) and entropy-enriched flux tubes [*Wolf et al.*, 2009]. However, in that case, the subsequent treatment by ideal MHD seems questionable, particularly for the blob, within which the equatorial magnetic field strength gets further reduced, a main reason for the break-down of ideal MHD. Thus, the subsequent evolution might be better modeled by non-ideal approaches, which lead to reconnection and plasmoid ejection rather than a blob that remains connected to Earth.

[25] A more justifiable mechanism might be a sudden temperature increase, for instance from resonant wave absorption, which could even take the form of a thermal catastrophe, as suggested by *Smith et al.* [1986] and *Goertz and Smith* [1989], who proposed this as a substorm onset mechanism. The tailward motion of the blob and the formation of the more eminent region-2 type currents, however, are contrary to the expectations of the thermal catastrophe model, so that it does not seem a viable substorm onset model. In any case, the ionospheric connection via region-2 type currents might provide a remote possibility of identification of blobs, in contrast to disconnected plasmoids, whether they are related to substorms or not.

Appendix A: Effects of the Grid Resolution

[26] As mentioned above, the number of grid points and the resolution has no significant effect on the results demonstrated here. This is demonstrated by Figures A1, A2, and A3. Figure A1 shows the temporal evolution of field-aligned currents (maximum/minimum and integrated) at the inner boundary for two values of grid cells n_y in the y direction. Obviously, the higher resolution does not produce any significant change. The remainder of the runs therefore were done with the lower resolution.

[27] Figure A2 shows again the temporal evolution of field-aligned currents at the inner boundary for different

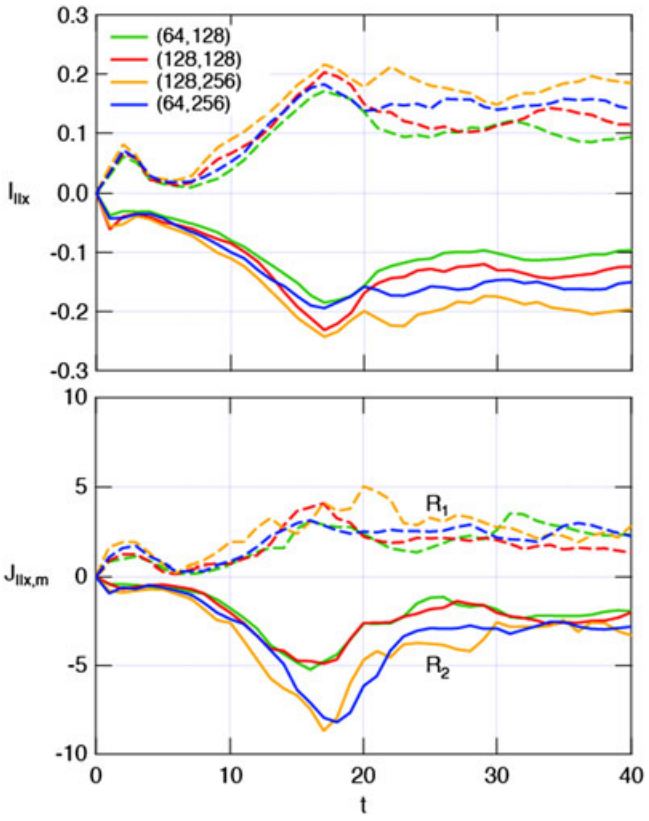

Figure A2. Temporal evolution of field-aligned currents at the near-Earth boundary $x = 0$ for $f = 2$, $n_y = 40$, and different numbers of grid cells (n_x, n_z) as indicated: (a) maximum and minimum current density $J_{\|x}$ and (b) total integrated current of region-1 and region-2 type.

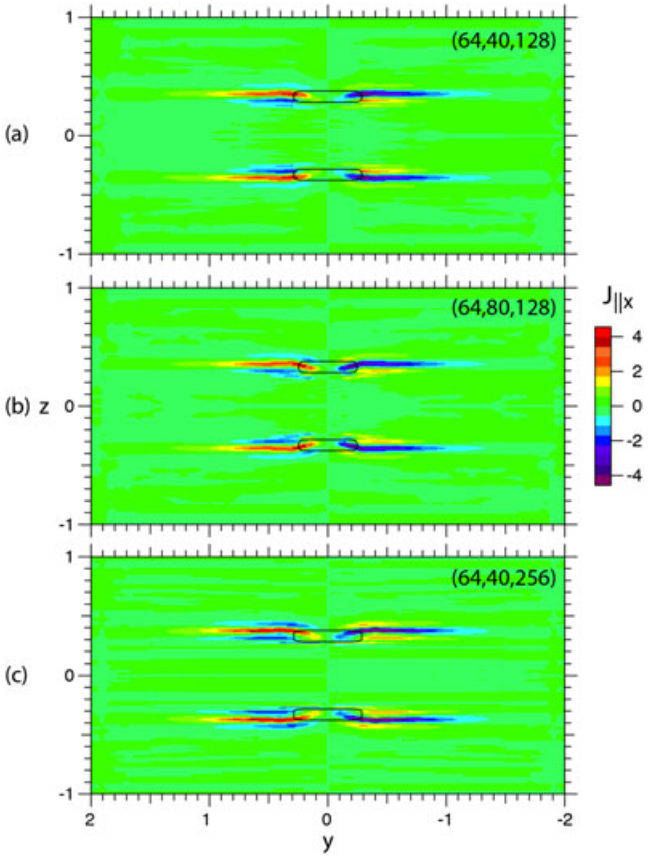

Figure A3. Field-aligned currents $J_{\|x}$ (color) at the inner boundary $x = 0$ at $t = 15$ for different resolution in x, y, and z, as indicated by the numbers of grid cells (n_x, n_Y, n_z). The black contours again outline the cross section of the flux tube with enhanced entropy.

values of grid cells n_x and n_z. The effects on the integrated currents are small. However, the maximum (negative) current density of region-2 type, which dominates the current pattern, increase with increasing resolution in z, whereas the effect on the more widely distributed region-1 type current density is small.

[28] Figure A3 further demonstrates that the field-aligned current pattern at $x = 0$ is not significantly affected at $t = 15$, which is close to the time the current densities and the integrated currents reach their maximum. At later times, however, the stopping of the flows and the increasing turbulence cause more highly structured current patterns in the more highly resolved runs, not shown here.

[29] **Acknowledgments.** This work was performed mainly at Los Alamos under the auspices of the US Department of Energy, supported by NSF's GEM and NASA's MMS/SMART Theory and Modeling and SR&T Programs. We thank both referees for stimulating "minor" comments and questions.

[30] Robert Lysak thanks Joachim Raeder and another reviewer for their assistance in evaluating this paper.

References

Angelopoulos, V., W. Baumjohann, C. F. Kennel, F. V. Coroniti, M. G. Kivelson, R. Pellat, R. J. Walker, H. Lühr, and G. Paschmann (1992), Bursty bulk flows in the inner central plasma sheet, *J. Geophys. Res.*, *97*, 4027.

Angelopoulos, V., et al. (1994), Statistical characteristics of bursty bulk flow events, *J. Geophys. Res.*, *99*, 21,257–21,280.

Baumjohann, W., G. Paschmann, and H. Lühr (1990), Characteristics of high-speed ion flows in the plasma sheet, *J. Geophys. Res.*, *95*, 3801.

Birn, J., F. Iinoya, J. U. Brackbill, and M. Hesse (1996), A comparison of MHD simulations of magnetotail dynamics, *Geophys. Res. Lett.*, *23*, 323.

Birn, J., J. Raeder, Y. L. Wang, R. A. Wolf, and M. Hesse (2004), On the propagation of bubbles in the geomagnetic tail, *Ann. Geophys.*, *22*, 1773.

Birn, J., M. Hesse, K. Schindler, and S. Zaharia (2009), Role of entropy in magnetotail dynamics, *J. Geophys. Res.*, *114*, A00D03, doi:10.1029/2008JA014015.

Book, D. L., J. P. Boris, and K. Hain (1975), Flux corrected transport II: Generalizations of the method, *J. Comp. Phys.*, *18*, 248.

Chen, C. X., and R. A. Wolf (1993), Interpretation of high-speed flows in the plasma sheet, *J. Geophys. Res.*, *98*(21), 409.

Chen, C. X., and R. A. Wolf (1999), Theory of thin-filament motion in Earth's magnetotail and its application to bursty bulk flows, *J. Geophys. Res.*, *104*(14), 613.

Dubyagin, S., V. Sergeev, S. Apatenkov, V. Angelopoulos, A. Runov, R. Nakamura, W. Baumjohann, J. McFadden, and D. Larson (2011), Can flow bursts penetrate into the inner magnetosphere?, *Geophys. Res. Lett.*, *38*, L08102, doi:10.1029/2011GL047016.

Fairfield, D. H., et al. (1999), Earthward flow bursts in the inner magnetotail and their relation to auroral brightenings, AKR intensifications, geosynchronous particle injections and magnetic activity, *J. Geophys. Res.*, *104*, 355.

Forsyth, C., et al. (2008), Observed tail current systems associated with bursty bulk flows and auroral streamers during a period of multiple substorms, *Ann. Geophys.*, *26*(1), 167–184.

Fuchs, K., and G.-H. Voigt (1979), *Self-consistent Theory of a Magnetospheric B-field Model, in Quantitative Modeling of Magnetospheric Processes*, in *Geophys. Monogr.,* vol. 21, edited by W. P. Olson, p. 86, Am. Geophys. Union, Washington, D. C.

Goertz, C. K., and W. Baumjohann (1991), On the thermodynamics of the plasma sheet, *J. Geophys. Res.*, *96*, 20,991–20,998.

Goertz, C. K., and R. A. Smith (1989), The thermal catastrophe model of substorms, *J. Geophys. Res.*, *94*, 6581–6596.

Grocott, A., T. K. Yeoman, R. Nakamura, S. W. H. Cowley, H. U. Frey, H. Rème, and B. Klecker (2004), Multi-instrument observations of the ionospheric counterpart of a bursty bulk flow in the near-Earth plasma sheet, *Ann. Geophys.*, *22*, 1061–1075.

Hones, E. W. J. (1977), Substorm processes in the magnetotail: Comments on 'On hot tenuous plasma fireballs and boundary layers in the Earth's magnetotail' by L. A. Frank, K. L. Ackerson, and R. P. Lepping, *J. Geophys. Res.*, *82*, 5633.

Hu, B., R. A. Wolf, F. R. Toffoletto, J. Yang, and J. Raeder (2011), Consequences of violation of frozen-in-flux: Evidence from OpenGGCM simulations, *J. Geophys. Res.*, *116*, A06223, doi:10.1029/2011JA016667.

Lee, L. C., L. Zhang, A. Otto, G. S. Choe, and H. J. Cai (1998), Entropy antidiffusion instability and formation of a thin current sheet during geomagnetic substorms, *J. Geophys. Res.*, *103*(A12), 29,419–29,428, doi:10.1029/97JA02141.

Lui, A. T. Y., et al. (1992), Current disruptions in the near-Earth neutral sheet region, *J. Geophys. Res.*, *97*, 1461–1480, doi:10.1029/91JA02401.

Lyons, L. R., T. Nagai, G. T. Blanchard, J. Samson, T. Yamamoto, T. Mukai, A. Nishida, and S. Kokubun (1999), Association between geotail plasma flows and auroral poleward boundary intensifications observed by canopus photometers, *J. Geophys. Res.*, *104*, 4485.

Nagai, T., et al. (1998), Structure and dynamics of magnetic reconnection for substorm onsets with Geotail observations, *J. Geophys. Res.*, *103*, 4419–4440.

Nakamura, R., W. Baumjohann, M. Brittnacher, V. A. Sergeev, M. Kubyshkina, T. Mukai, and K. Liou (2001a), Flow bursts and auroral activations: Onset timing and foot point location, *J. Geophys. Res.*, *106*, 10,777–10,789.

Nakamura, R., W. Baumjohann, R. Schödel, M. Brittnacher, V. A. Sergeev, M. Kubyshkina, T. Mukai, and K. Liou (2001b), Earthward flow bursts, auroral streamers, and small expansions, *J. Geophys. Res.*, *106*, 10,791–10,802.

Øieroset, M., T. D. Phan, R. P. Lin, and B. U. Ö. Sonnerup (2000), Walén and variance analyses of high-speed flows observed by wind in the mid-tail plasma sheet: Evidence for reconnection, *J. Geophys. Res.*, *105*(25), 247.

Petrukovich, A. A., W. Baumjohann, R. Nakamura, R. Schödel, and T. Mukai (2001), Are earthward bursty bulk flows convective or field-aligned? *J. Geophys. Res.*, *106*, 21,211–21,215.

Pontius, D., and R. A. Wolf (1990), Transient flux tubes in the terrestrial magnetosphere, *Geophys. Res. Lett.*, *17*, 49.

Schödel, R., W. Baumjohann, R. Nakamura, V. Sergeev, and T. Mukai (2001a), Rapid flux transport in the central plasma sheet, *J. Geophys. Res.*, *106*, 301.

Schödel, R., R. Nakamura, W. Baumjohann, and T. Mukai (2001b), Rapid flux transport and plasma sheet reconfiguration, *J. Geophys. Res.*, *106* (83), 811.

Sergeev, V., R. C. Elphic, F. S. Mozer, A. Saint-Marc, and J.-A. Sauvaud (1992), A two-satellite study of nightside flux transfer events in the plasma sheet, *Planet. Space Sci*, *40*, 1551–1572.

Sergeev, V., K. Liou, P. T. Newell, S.-I. Ohtani, M. R. Hairston, and F. Rich (2004), Auroral streamers: Characteristics of associated precipitation, convection and field-aligned currents, *Ann. Geophys. Res.*, *22*, 537.

Sergeev, V. A., V. Angelopoulos, J. T. Gosling, C. A. Cattell, and C. T. Russell (1996), Detection of localized, plasma-depleted flux tubes or bubbles in the midtail plasma sheet, *J. Geophys. Res.*, *101*, 10,817–10,826, doi:10.1029/96JA00460.

Shay, M. A., J. F. Drake, M. Swisdak, W. Dorland, and B. N. Rogers (2003), Inherently three dimensional magnetic reconnection: A mechanism for bursty bulk flows? *Geophys. Res. Lett.*, *30*, 345–348, doi:10.1029/2002GL016267.

Smith, R. A., C. K. Goertz, and W. Grossman (1986), Thermal catastrophe in the plasma sheet boundary layer, *Geophys. Res. Lett.*, *13*, 1380–1383.

Wolf, R. A., Y. Wan, X. Xing, J.-C. Zhang, and S. Sazykin (2009), Entropy and plasma sheet transport, *J. Geophys. Res.*, *114*, A00D05, doi:10.1029/2009JA014044.

Yang, J., F. R. Toffoletto, G. M. Erickson, and R. A. Wolf (2010a), Superposed epoch study of $PV^{5/3}$ during substorms, pseudobreakups and convection bays, *Geophys. Res. Lett.*, *37*, L07102, doi:10.1029/2010GL042811.

Yang, J., R. A. Wolf, and F. R. Toffoletto (2010b), Accelerated thinning of the near-Earth plasma sheet caused by a bubble-blob pair, *Geophys. Res. Lett.*, *38*, L01107, doi:10.1029/2010GL045993.

Zesta, E., L. R. Lyons, and E. Donovan (2000), The auroral signature of earthward flow bursts observed in the magnetotail, *Geophys. Res. Lett.*, *27*, 3241–3244.

Zhu, P., J. Raeder, C. C. Hegna, and C. R. Sovinec (2013), Nature of axial tail instability and bubble-blob formation in near-Earth plasma sheet, *J. Geophys. Res. Space Physics*, *118*(2), 653–663, doi:10.1029/2012JA017972.